Effect of cytoskeletal geometry on intracellular diffusion

J. J. Blum,* G. Lawler, M. Reed, and I. Shin
*Division of Physiology, Department of Cell Biology, and Department of Mathematics, Duke University, Durham, North Carolina 27706

ABSTRACT A method is presented for determining the retardation of diffusion of particles inside cells owing to cytoskeletal barriers. The cytoskeletal meshwork is treated as a repeating periodic two-dimensional or three-dimensional lattice composed of elements of given size, shape, and spacing. We derive an analytic expression for the diffusion coefficient relative to that of the cytosol. This expression is evaluated by solving numerically an appropriate boundary-value problem for the Laplace equation. For the two-dimensional case, e.g., diffusion in a membrane, the results are quantitatively similar to those obtained by Saxton (1987. *Biophys. J.* 52:989–997) using Monte Carlo methods. The three-dimensional results are quantitatively similar to experimental results reported by Luby-Phelps et al. (1987. *Proc. Natl. Acad. Sci. USA.* 84:4910–4913) for the diffusion of dextran and Ficoll particles in Swiss 3T3 cells. By accounting for geometrical factors, these results allow one to assess the relative contributions of geometrical hindrance and of binding to the cytoskeletal lattice from measurements of intracellular diffusion coefficients of proteins.

INTRODUCTION

Measurements of the intracellular diffusion coefficients of small molecules indicate that the viscosity of the aqueous portion of the cytoplasm generally ranges from two- to at most sixfold that of water (Mastro et al., 1984; Jacobson and Woijcieszyn, 1984; Luby-Phelps et al., 1988). Larger particles, such as proteins or dextrans, however, diffuse much more slowly than could be accounted for by this relatively small increase in cytosolic viscosity (reviewed in Luby-Phelps et al., 1988). It is well established that the interior of most cells contains an extensive latticework of cytoskeletal elements; in cultured PTK cells, for example, Gershon et al. (1985) estimated that this cytoplasmic matrix occupies from 16% to 21% of the available volume. They suggested that nonspecific binding of proteins to the cytoskeletal elements largely accounts for the very low, and often size-independent (Jacobson and Woijcieszyn, 1984) diffusion coefficients measured for proteins inside intact cells. For quantitative understanding of the observed low diffusion coefficients, it is also necessary to take into account the retardation of diffusion owing to the cytoskeletal barriers that will occur even in the absence of binding.

Evidence for the retardation of diffusion due to cytoskeletal barriers comes from several experiments. When cells are exposed to hypertonic solutions, the volume decrease causes a decrease in spacing between elements of the cytoskeletal network and both small molecules (Mastro et al., 1984) and proteins (Jacobson and Woijcieszyn, 1984) diffuse much more slowly. Luby-Phelps et al. (1986, 1987) have shown that fluorescein isothiocyanate-labeled dextrans, which do not bind to the cytoskeleton, have intracellular mobilities that vary inversely with molecular size. Indeed, their measurements indicate that for proteins with a diameter exceeding 26 nm size is as important a factor in determining cytoplasmic diffusibility as binding.

The relative importance of binding (specific or nonspecific) to the cytoskeletal matrix and hindrance to diffusion caused by the latticework will vary depending on the state of the cell since the organization and spacing of the cytoskeleton is a dynamic property. An "extreme" case of reorganization occurred in the experiments of Kempner and Miller (1968) in which the cell contents were stratified as a result of centrifugation. The supernatant cytosol was virtually free of protein. This finding was interpreted to mean that the cytosolic proteins were associated with large particulates or were bound to a structural system that sedimented rapidly. Some of the effect could, however, also be due to trapping of proteins in the compressed cytoskeletal meshwork.

The effect of the binding of proteins to the cytoskeleton on the effective diffusion coefficient can be computed straightforwardly from an estimate of the binding constant (Gershon et al., 1985). Analysis of the effect of the geometrical organization of the cytoskeleton, however, is a formidable problem since many factors, e.g., the volume excluded, lattice spacing, or geometry of the lattice elements, will affect the diffusion coefficient. Some

related work has been done by Saxton (1987, 1988), who considered lateral diffusion of mobile proteins in a membrane with either mobile or immobile obstacles (i.e., the two-dimensional case). His Monte Carlo calculations showed that the obstruction effect accounts for about half of the observed decrease in diffusion coefficient and that the magnitude of the effect was not strongly dependent on the geometrical organization of the obstructions.

In this article we investigate the effect of the cytoskeletal structure on the diffusion of particles such as dextrans or Ficoll, which do not bind to the lattice, and use the results to reexamine published experimental data. Because of the mathematical difficulty of dealing with the complexity of organization of real cytoskeletal lattices, we assume for simplicity that the meshwork is a three-dimensional periodic cubic lattice. Even though cytoskeletal lattices are neither cubic nor periodic, this is a reasonable approach to get a first approximation of the retardation of diffusion as a function of particle size, lattice spacing, and obstacle geometry. Our method is to derive an analytic expression for the diffusion coefficient in the presence of obstacles in terms of a solution of the Laplace equation with appropriate boundary conditions. This elliptic boundary value problem is then solved by standard numerical techniques. Details of the mathematical and computational methods are given in Appendixes 1 and 2, respectively. These techniques are used to evaluate the effective diffusion coefficients of inert particles of various sizes in two- and three-dimensional lattices of specified geometry. Finally, we discuss the relative contributions, under various physiological conditions, of viscosity, binding, and geometrical hindrance, to the retardation of diffusion inside cells.

METHODS

The arrangement of cytoskeletal elements in cells varies with cell type but within each cell a more or less regular latticework is discernible. On a microscopic scale, however, spacing between adjacent elements may vary considerably. Furthermore, the size and shapes of the elements will also vary; e.g., microtubules, intermediate filaments, and actin microfilaments have different diameters. Even if one had precise knowledge of the distribution of size and shape for the lattice elements in a particular cell, the mathematical and numerical difficulties in computing a local diffusion coefficient would be enormous. Furthermore, such calculations would not be particularly useful since the effective diffusion coefficient would vary from place to place in the particular cell (see, for example, Luby-Phelps and Taylor, 1988) and would give little information about other cells even for cells of the same type. Diffusion coefficients are measures of average properties of a system. Therefore, as a first approximation, it is reasonable to treat the latticework as though it were made up of elements of uniform size arranged in a periodic fashion.

We denote by D_w the diffusion coefficient for a particle of radius r in water, and by D_g the diffusion coefficient for the same particle diffusing in water past periodic obstructions of specified geometry. D_g will depend on the shape and size, r_o, of the obstructions. These parameters are illustrated in Fig. 1 *A* for the case of circular particles and circular obstructions in two dimensions. D_g would be the same for a point particle ($r = 0$) diffusing among circular obstacles of radius $r_o + r$, as shown in Fig. 1 *B*.

$$D_g(r, L, r_o) = D_g(0, L, r_o + r).$$

If the particles or obstacles are not circular, then this equality will not be exact but $D_g(0, L, r_o + r)$ will be a very good approximation to $D_g(r, L, r_o)$. The diffusion coefficient $D_g(0, L, r_o + r)$ does not change if we take $L = 1$ and scale the size of the obstacles accordingly (see Fig. 1 *C*):

$$D_g(0, 1, (r_o + r)/L) = D_g(0, L, r_o + r).$$

We denote $(r_o + r)/L$ by c.

We now state a theorem which allows one to express the diffusion coefficient, D_g, in terms of the solution to an elliptic boundary value problem. Actually, we state the special isotropic case here, since that is what is used in the subsequent calculations in this article. The general

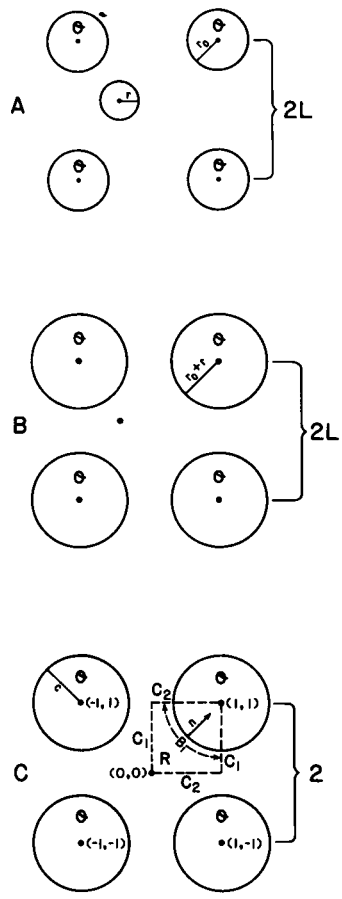

FIGURE 1 Diffusion in two dimensions past circular obstacles. (*A*) A spherical particle of radius r diffuses among a periodic array (period $2L$) of circular obstacles (labeled) ⊘ of radius r_o. (*B*) A point particle diffuses among a periodic array of circular obstacles of radius $r_o + r$. (*C*) The fundamental domain for the elliptic boundary value problem is the region R bounded by the sides labeled C_1, C_2, and the curve B_1. The coordinates of the centers of the obstacles are given in parentheses.

case is stated in Appendix 1 where a sketch of the proof is given. The result is presented for diffusion in m dimensional space, $m \geq 2$, so it applies simultaneously to the cases $m = 2$ and $m = 3$ that are of interest here.

Consider a three-dimensional closed set (i.e., an object which is the obstacle to diffusion), $\mathcal{O}_0$, localized entirely within a cube centered at $x = y = z = 0$, so that $\mathcal{O}_0$ does not contain the point $x = y = z = -1$. Assume that $\mathcal{O}_0$ is symmetric under reflections along each axis, is invariant under a 90° rotation about the x, y, or z axes, and that $\mathcal{O}_0$ has piecewise smooth boundary (see Figs 2 and 3 for examples). Let $\mathcal{O}_1$ denote the set of points obtained by centering $\mathcal{O}_0$ at $x = y = z = 1$ instead of $x = y = z = 0$, and let $\mathcal{O}$ denote the two-periodic extension of $\mathcal{O}_1$ along every axis. That is, $x \in \mathcal{O}$ if and only if $x = y + (2j_1, 2j_2, \ldots, 2j_3)$ for some point y in $\mathcal{O}_1$ and integers j_1, j_2, j_3. $\mathcal{O}$ is then the region excluded for the diffusion of particles. (The extension of this derivation to objects in m-dimensional space is self-evident, as is the reduction to two dimensions.)

Let Q_1 be the unit cube $\{\vec{x} | 0 \leq x_i \leq 1\}$ and let the fundamental domain R consist of the remaining points of Q_1 after points in $\mathcal{O}_1$ have been removed. R is the fundamental subregion available for diffusion. We assume that the boundary of $\mathcal{O}_1$ in Q_1 is smooth and we denote it by B_1. Let

$$C_i = \{\vec{x} \in R | x_i = 0 \text{ or } x_i = 1\}$$

The C_i are the parts of the faces of Q_1 which are not in $\mathcal{O}_1$. With this notation we can now state:

Theorem (isotropic case). Suppose that the diffusion in R^m with coefficient D is retarded by the obstacles $\mathcal{O}$. Let $n = (n_1, n_2, \ldots, n_m)$ be the normal on B_1, pointing into $\mathcal{O}_1$, and let $w(x)$ be the solution to the elliptic boundary value problem:

$$(a)\ \nabla^2 w(x) = 0 \qquad x \in R$$

$$(b)\ \frac{\partial w}{\partial n} = n_1 \qquad x \in B_1$$

$$(c)\ w(x) = 0 \qquad x \in C_1$$

$$(d)\ \frac{\partial w}{\partial n}(x) = 0 \qquad x \in C_i,\ i \neq 1$$

Then the effective diffusion coefficient is given by

$$D_g = \left\{1 - (\text{vol}(R))^{-1} \int_{B_1} w n_1 ds\right\} D,$$

where S is surface measure on B_1.

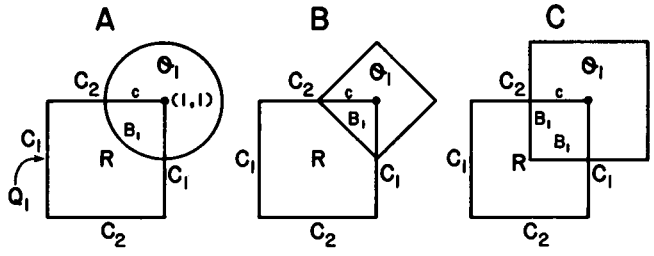

FIGURE 2 The region R in two dimensions. The region R and the boundary B_1 are shown for the cases of circular, dimaond-shaped, and square obstacles, in two dimensions. R consists of the points in the square Q_1 which are not in the obstacle $\mathcal{O}_1$.

The boundary conditions (c and d) arise from simple symmetry considerations. The essence of the theorem is that the solution of the Laplace equation with boundary conditions (b) yields the correct diffusion coefficient via the above formula. The proof, which is nontrivial, is sketched in Appendix 1.

Figs. 2 and 3 give examples of the regions R and the boundary B_1 in two and three dimensions. The point of the theorem is that it gives an explicit analytical expression for the effective diffusion constant in terms of w, the solution to an elliptic boundary value problem. This is useful for two reasons. First, the explicit expression allows one to prove estimates comparing various cases (see, for example, Shin, Ph.D. thesis, in preparation). Secondly, the numerical analysis of elliptic boundary value problems has been thoroughly studied, so one can use standard procedures and software packages to get highly accurate values for D_g in a wide range of geometric situations.

RESULTS

We begin with results obtained for a two-dimensional lattice since the geometry is much easier to visualize than in three dimensions and much can be learned that applies to the three-dimensional case. Furthermore, these two-dimensional calculations may be applicable to diffusion in membranes. Since microtubules are ~24 nm in diameter, intermediate filaments are ~7–11 nm and actin microfilaments ~4–6 nm, simulations were run with 5- and 10-nm beam radii. Typical lattice spacings in the cytoskeletal meshwork are of the order of 100 nm (Gershon et al., 1985), so we have chosen to examine diffusion in lattices of 60-, 100-, and 140-nm lattice spacing for each beam size. Figs. 4 and 5 show the ratio of D_g to D_w for particles of different sizes obtained by numerical computation using the methods described in detail in Appendix 2.

For a particle diffusing among periodic circular obstacles, particle size will have a dramatic effect when particle size approaches interobstacle distance. This is expected since the particle becomes effectively trapped when its diameter approaches the size of the available

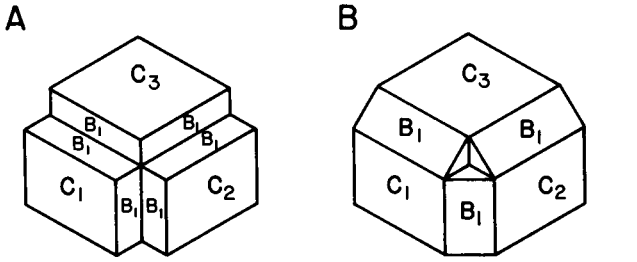

FIGURE 3 The region R and the surfaces B_1 in three dimensions. The region R and the surface boundary B_1 are shown for a cubic lattice of beams with (A) square and (B) diamond-shaped cross section, in three dimensions. So that the B_1 surfaces can be seen, the figures are depicted as they would be seen looking back along the line $x = y = z$ toward the origin. C_1, C_2, and C_3 are the parts of the faces of the cube, Q_1, that are not in the beams, $\mathcal{O}_1$.

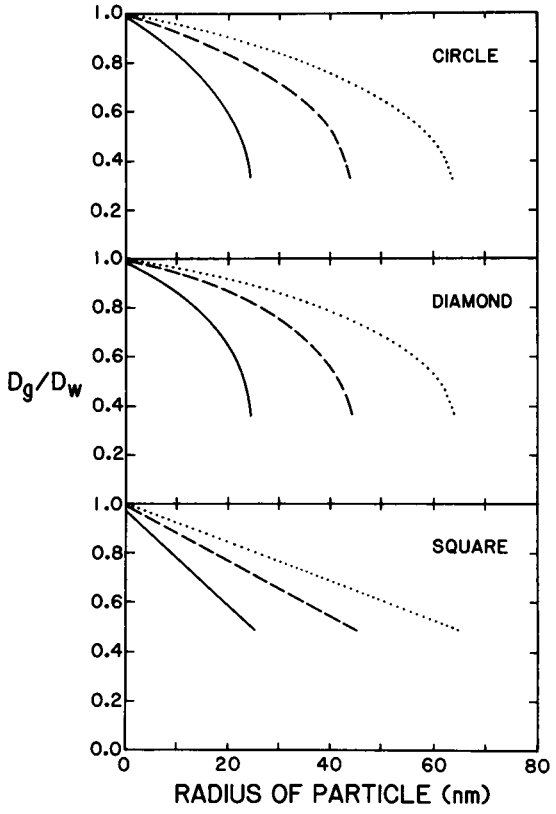

FIGURE 4 Diffusion in a periodic two-dimensional lattice. The ratio D_g/D_w is shown as a function of particle radius for a two-dimensional array of periodic obstacles of circular, diamond, and square shapes, each 5 nm in radius. Lattice spacings are 60 nm (*solid line*); 100 nm (*dashed line*); 140 nm (*dotted line*).

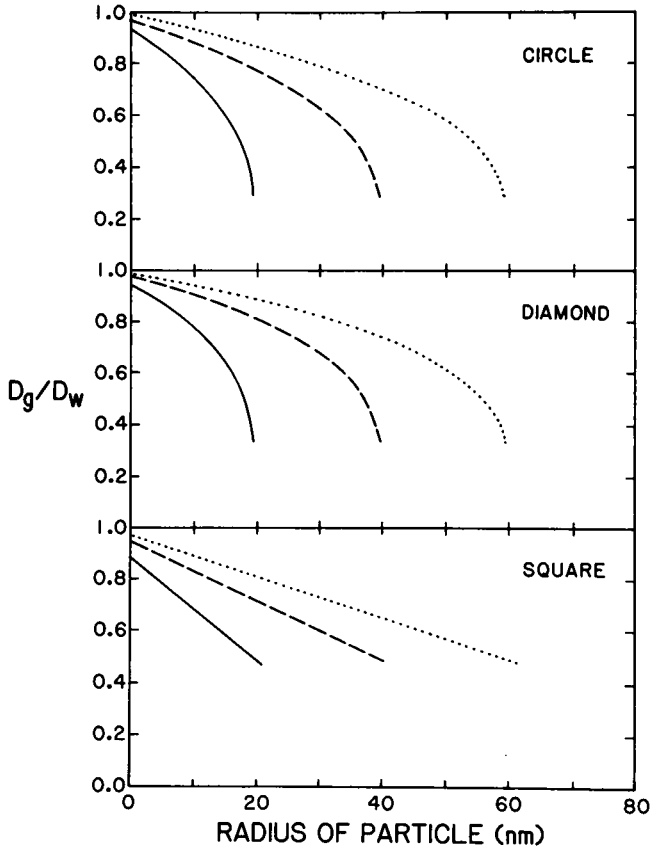

FIGURE 5 Diffusion in a periodic two-dimensional lattice. The parameters are the same as in Fig. 4 except that the radius of the obstacles is 10 nm.

openings between obstacles. For lattice spacing 60 nm and obstacle radius 5 nm, the critical radius is 25 nm (Fig. 4). For both circular and diamond-shaped obstacles, D_g falls slowly until the particle radius is within ~5 nm of the critical radius, after which it falls precipitously.

Notice that the case of square obstacles is somewhat different. As the particle radius approaches the critical radius, D_g does not approach zero, but approaches 0.5. It is easy to see that D_g is always ≥ 0.5 since at all times the particle is free to diffuse in one of the two coordinate directions. As the particle radius approaches the critical size, the particle is effectively constrained to move in long, narrow regions in which it can diffuse horizontally or vertically, but not both. The fact that $D_g \rightarrow 0.5$ can be proven analytically. In the circular and diamond-shaped cases, however, there remains a residual area within each of the repeating lattice domains in which the particle can diffuse locally. Therefore the probability that it will move along one of the vertical or horizontal channels into the next domain approaches zero as particle radius approaches the critical limit. This shows that, from the mathematical point of view, there are subtle and interesting effects of the geometry on the diffusion near the critical radius. This is also true in three dimensions.

From the biological point of view these subtleties are irrelevant because the simplifying assumptions used break down near the critical size. First, cytoskeletal lattices are not regularly repeating structures and therefore there is a range of "critical" sizes. Secondly, the cytoskeletal elements are certainly not regular geometric shapes. Thirdly, the assumption that the diffusion of a finite size particle in a lattice is approximately the same as that of a point particle in a lattice with correspondingly larger obstacles breaks down near the critical radius. Finally, implicit in our treatment is the assumption that the mobility tensor is scalar, i.e., that particle mobility is independent of direction and position. In a narrow pore, however, hydrodynamic effects will certainly play a role (see Renkin, 1955). Furthermore, close to the obstacle the hydrodynamic properties of the cytosol itself may change (i.e., bound water; see Luby-Phelps and Taylor, 1988). These hydrodynamic effects will be of significance when particle size approaches the critical radius. Therefore,

when discussing the diffusion of proteins and dextran particles in cells, the calculations in Figs. 4 and 5 (and 6 and 7 below) are used only for particles appreciably smaller than the critical size. Notice that for particles whose radii are $<\sim 75\%$ of the critical size, the curves for circular, diamond-shaped, and square obstacles are very similar (Fig. 4). Thus the precise shapes of the obstacles have very little influence on the effective diffusion coefficient away from the critical size.

It should be noted that as the particle radius approaches zero, the ratio D_g/D_w remains less than unity. This is because the obstacles occupy a finite percentage of the available area for diffusion, which in itself reduces the diffusion coefficient slightly. As expected, the effect is greater as the lattice spacing decreases because the percentage of excluded area is greater. Also, this effect increases with increasing obstacle diameter for a given lattice spacing (compare Figs. 4 and 5). Except for this, there is very little qualitative or quantitative difference between the curves for D_g/D_w in the 10- and 5-nm obstacle size cases. Thus, for a given lattice spacing, neither obstacle size (up to 10-nm radius) nor shape has a major influence on D_g.

The results for diffusion in a three-dimensional periodic lattice are presented in Figs. 6 and 7 for the cases of beams with square and diamond-shaped cross sections, respectively. We did not include circular cross-sections since the curved boundaries make the numerical analysis more difficult and, based on our two-dimensional work, we did not expect the results to differ appreciably from

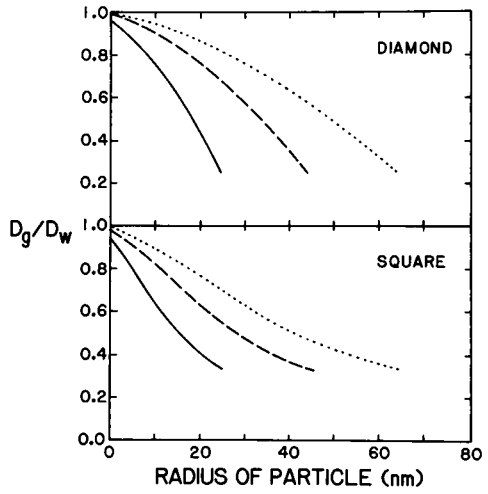

FIGURE 6 Diffusion in a periodic three-dimensional lattice. The ratio D_g/D_w as a function of particle size for diffusion through a cubic latticework of beams with diamond-shaped and square cross sections and 5 nm in radius is shown for assumed lattice spacings of 60 nm (*solid line*), 100 nm (*dashed line*), and 140 nm (*dotted line*), respectively. All the parameters are the same for beams with square cross sections.

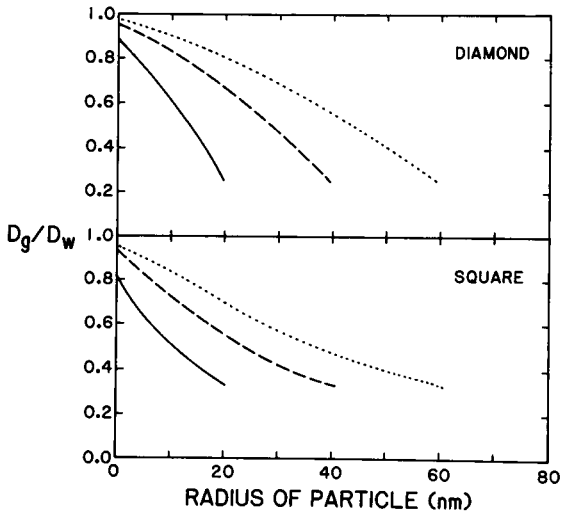

FIGURE 7 Diffusion in a periodic three-dimensional lattice. All parameters are the same as in Fig. 6 except that the radius of the cross section of the beams is 10 nm.

the diamond-shaped case. The general pattern is similar to the two-dimensional cases discussed above. Notice that, for beams of a square cross section, the limit of D_g/D_w as particles approach the critical radius is one-third, as expected since the diffusion of such particles will be effectively constrained to one-dimensional diffusion in one of the three coordinate axes. For a diamond-shaped cross section, the ratio D_g/D_w decreases and presumably approaches zero as the radius approaches critical size because of the residual volume. We have not been able to prove this analytically but the numerical evidence indicates that if $D_g/D_w \rightarrow 0$ the drop is precipitous in the last 0.1% of the gap size. Note also that the excluded volume effect as particle size goes to zero is larger than in the two-dimensional case (compare Figs. 6 and 7 with Figs. 3 and 4, respectively). For example, letting c be as indicated in Appendix 2, the excluded area in the square obstacle cases is c^2 while the excluded volume in the case of beams with square cross section is $3c^2 - 2c^3$. Thus for small c the excluded region is larger for the three-dimensional than for the two-dimensional case. As expected from the two-dimensional results, the effects of beam size and geometry are not very important for particles appreciably smaller than the critical size.

DISCUSSION

Interest in the effects of periodically arranged obstacles on the conductivity of heat or electricity goes back at least to Lord Rayleigh (Rayleigh, 1892). He derived approximate expressions for the conductivity for low area circular

or low volume spherical obstacles. Since that time much has been done on low volume approximations. The analytical expression that we have derived (Appendix 1, Eq. 4) is valid for obstacles of general shape and size up to the critical radius. The amount of numerical calculation required to solve the elliptic boundary value problem to any degree of accuracy needed and to obtain a numerical value for the expression will depend on the geometry of the obstacle. Although the mathematical and numerical treatment is valid up to the critical radius, the biological assumptions become inappropriate near the critical radius.

It is generally accepted that neither dextran nor Ficoll particles bind appreciably to the cytoskeleton (Luby-Phelps et al., 1987), and therefore they have been used as probes of cytoskeletal structure. In order to compare our theoretical predictions with experiments one has to take into account the fact that the aqueous phase of the cytoplasm has a viscosity, η, two to six times that of water. Taking, for example, $\eta = 4$ cp (Luby-Phelps et al., 1986), the effective diffusion coefficient, D_{eff}, for dextran or Ficoll particles is $D_{eff} = D_g/4$. Thus the theoretical predictions for D_{eff} can be obtained from Figs. 4 and 5 merely by dividing the ordinate values by 4 to enable these values to be compared to those obtained for the Swiss 3T3 cells used in the studies of Luby-Phelps et al. (1987). These predictions are in good qualitative agreement with the intracellular diffusion values obtained by Luby-Phelps et al. (1987, their Fig. 1) for both dextran and Ficoll particles. They found that as particle radius approaches zero, D_{eff}/D_w approaches ~0.24 for dextran and 0.32 for Ficoll. With increasing particle size, D_{eff}/D_w for Ficoll decreases steadily until the radius approaches 26 nm at which size most of the particles are immobile. Assuming a beam radius of 5–10 nm, our calculations indicate an average lattice spacing ranging from 62 (Fig. 6) to 72 (Fig. 7) nm. We remark that the "radius" used by Luby-Phelps et al. (1987, 1988) to describe particle size is the radius of gyration which will typically underestimate somewhat a true maximal half-diameter of the particle. Thus the critical radius is probably somewhat >26 nm, and the lattice spacing is likely to be somewhat larger than the range 62–72 nm. In PTK and NRK cells, the average size of pores in the cytoskeletal lattice has been estimated to range from 72 to 98 nm (Gershon et al., 1983).

Figs. 6 and 7 show that for beams with diamond-shaped cross sections D_g decreases almost linearly with increasing particle size for particles well below the critical size. Similarly, an approximately linear decline in diffusion coefficient was measured for both Ficoll and dextran particles (Luby-Phelps et al., 1987). Furthermore, the slopes of the linear regions are comparable when a factor of 3 to 4 is used for the ratio of cytoplasmic viscosity to that of water. This supports the idea that computations based on periodic lattices are a reasonable first approximation for understanding the retardation of diffusion owing to geometry. Of course, for large particle sizes the nonperiodicity of the cellular lattice will cause greater differences between theory and experiment. In our calculations, there is a sharp cutoff at the critical size. In real cells, there will be some trapping below the average critical size and some freedom above the critical size. Indeed, such freedom above the critical size was observed by Luby-Phelps et al. (1987).

Several authors have conducted experiments in which the intracellular diffusion coefficients of various proteins were determined. Jacobson and Woijcieszyn (1984) observed that the diffusion coefficients of macromolecules with radii ranging from ~0.6 to 6 nm were close to 10^{-8} cm^2/s and concluded that diffusion in the cells was dominated by binding to elements of the cytomatrix and that steric effects played only a small role. Our calculations (see Fig. 7), show that for particles in this size range very little hindrance to diffusion will occur for lattice spacing greater than, say, 60 nm. This supports their conclusion that binding is the dominant effect for these proteins. Mastro et al. (1984) showed that for very small nonbinding molecules (radius ~0.3 nm) viscosity is the major determinant of particle movement under physiological conditions. However, when cells were subjected to hypertonic conditions a marked reduction in the diffusion coefficient was detected. Our calculations show that for beam radii in the 5–10-nm range one would have to have lattice spacings as small as 10–15 nm to noticeably impede diffusion of a molecule of radius 0.3 nm. This spacing is much smaller than would be expected owing to the shrinking of the original lattice accompanying a 50% reduction in cell volume. The theoretical calculations therefore support the conclusions of Mastro et al. (1984) that new, closely spaced, cytoskeletal elements or their equivalent must appear under hypertonic conditions. Jacobson and Woijcieszyn (1984) also measured diffusion under hypertonic conditions and found that serum albumin became completely trapped. This is to be expected since for a lattice spacing of 10–15 nm, the radius of serum albumin, 3.6 nm, is close to the critical size where the diffusion coefficient drops precipitously (see, for example, Fig. 5). Under such hypertonic conditions, however, local regions of very high protein concentration might occur. As shown by O'Leary (1987) and by Muramatsu and Minton (1988), diffusion of proteins may be dramatically reduced if the protein concentration is high enough. This effect may also contribute to retardation under hypertonic conditions.

Gershon et al. (1985) investigated the retardation of diffusion of proteins through the cytoplasmic matrix. They assumed that for the cells with which they were

dealing (PTK cells), whose pore size is ~100 nm, geometrical hindrance played a negligble role and that the retardation was entirely (to a first approximation) due to the binding of proteins to the cytoskeleton. They derived the following formula:

$$D_{\text{eff}} = D_w(1 + K)^{-1},$$

relating the measured diffusion coefficient, D_{eff}, to the binding constant, K, of the protein to the cytoskeletal matrix. The effects of viscosity and of lattice size and spacing can be introduced into their formula as follows:

$$D_{\text{eff}} = \frac{D_g}{D_w}(1 + K)^{-1}\left(\frac{\eta_w}{\eta_c}D_w\right) = \frac{D_g}{D_w}(1 + K)^{-1}D_{\text{cyto}},$$

where η_w and η_c are the viscosities of water and the aqueous portion of the cytosol, respectively, and D_{cyto} is the diffusion coefficient for the particle under consideration in a fluid with the viscosity of the cytosol. D_g/D_w can be read off Fig. 5 for a given size particle and a given lattice spacing. Thus, if one has independent measurements of η_c, lattice geometry, particle size, and D_{eff}, then one can compute the effective intracellular binding constant, K, of the protein being studied to the cytoskeleton.

For PTK cells, fibroblasts, and similar cells where the lattice spacing is large, the factor D_g/D_w is close to 1 (Fig. 7) for almost all proteins since their radii are typically less than 6 nm (Jacobson and Woijcieszyn, 1984; Mastro et al., 1984). Nerve axons, however, are rich in neurofilaments, microtubules, and microfilaments (Ellisman and Porter, 1980). In a typical cross section of rat spinal nerve axons, for example, the average distance between microtubules is 107 nm and between neurofilaments is 49 nm (Gross and Weiss, 1982). Thus the average spacing between these lattice structures is <49 nm, say 40 nm. When account is taken of the presence of numerous microfilaments (Fath and Lasek, 1988) and of the many cross-bridges between these various filamentous structures, the effective lattice spacing could be quite small. This is consistent with the extremely small diffusion coefficients of fluorescein-labeled dextrans measured by Angelides (personal communication) in spinal cord axons. As mentioned above, lattice spacing may also be small enough under hypertonic conditions (Jacobson and Woijcieszyn, 1984; Mastro et al., 1984) to markedly retard diffusion.

Although our primary focus has been on diffusion inside of cells, the two-dimensional calculations are also of interest. Saxton (1987, 1989) has investigated the hindrance of diffusion of mobile proteins and lipids in membranes using a Monte Carlo simulation technique to calculate the effects of obstacle size and mobility on the diffusion coefficients of particles of various sizes and mobilities. Our approach is different in two respects. First, we consider a fixed periodic array of obstacles, whereas Saxton considers randomly arranged mobile obstacles. Secondly, he uses a discrete Monte Carlo simulation, whereas we use an analytic technique to reduce the problem to the solution of an elliptic boundary value problem which we then solve numerically. Despite these differences in assumptions and approach, the results are similar: away from the critical size, the details of the geometry are not very important but there is a size-dependent retardation of diffusion. Furthermore, the magnitude of the retardation effect is similar for the two approaches for particles and obstacles of comparable sizes. In certain cases, for example, coated pits, the assumption of regular periodic obstacles may be better than the assumption of randomly placed and moving obstacles.

A common assumption is that the area (or volume) fraction of the lattice of obstacles is the primary determinant of the retardation of diffusion. It is instructive, therefore, to replot our results in terms of area fraction. Fig. 8 shows the diffusion coefficient (relative to water) for a point particle diffusing in two dimensions among circular, square, and diamond-shaped obstacles. The lightly dotted line indicates the decrease one would observe if area fraction were the sole determinant of the retardation of diffusion. As expected all three curves lie along this dotted line for sufficiently small area fraction. D_g/D_w for square obstacles approaches 0.5 as the area fraction goes to 1 for reasons discussed above. D_g/D_w for diamond-shaped obstacles stays close to the dotted line until the area fraction 0.4 is reached after which it drops rapidly to zero because the diffusion becomes blocked at area fraction 0.5. For circular obstacles, D_g/D_w is higher than the dotted line because the circular shape facilitates

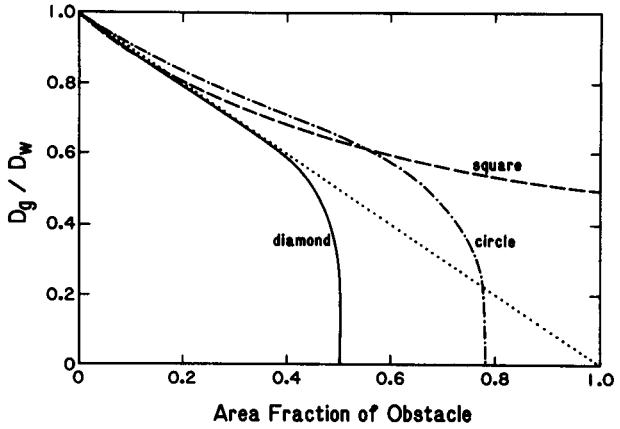

FIGURE 8 Diffusion coefficients for point particles diffusing in two-dimensional lattices consisting of circular, square, and diamond-shaped obstacles as a function of area fraction.

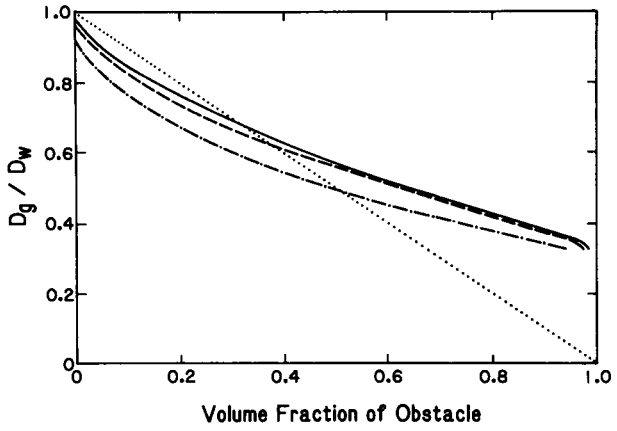

FIGURE 9 Diffusion coefficients for a spherical particle of radius 5 nm diffusing in a three-dimensional periodic lattice composed of beams of square cross section with lattice spacing of 60 nm (*dotted and dashed line*), 100 nm (*dashed line*), and 140 nm (*solid line*).

diffusion through the gaps between the obstacles. At sufficiently high area fraction, however, this effect is overcome by the blockage which occurs at area fraction $\pi/4$.

Fig. 9 shows the effect of lattice spacing for a particle of radius 5 nm diffusing among a three-dimensional latticework of beams of square cross section. At low volume fraction D_g/D_w is below the dotted line because the finite size of the particle is equivalent to a reduction of available volume. This effect, as described earlier, is larger for decreased lattice spacing. As the volume fraction increases, D_g/D_w approaches one-third, as expected. Figs. 8 and 9 show clearly that a range of other geometrical factors besides area or volume fraction influence the retardation of diffusion.

APPENDIX 1

Diffusion past periodic obstacles

We give here an outline of the proof of the theorem stated in the Methods. In fact, a somewhat more general theorem, which allows diffusion speeds to be different in different directions is presented. Details of the proof can be found in Shin, Ph.D. thesis, in preparation. For the case of a smooth boundary, another proof can be found in Vanninanthan (1981). We believe that the proof given here, which is based on ideas in Derrida (1983) and Derrida and Luck (1983) for the discrete case, is easier to understand.

We take a probabilistic view of diffusion. Let $X_t = (X_t^1, \ldots, X_t^m)$ be the position of a particle in m-dimensional space at time t. Then, the effective drift, μ, and the effective diffusion matrix, $\{\Sigma_{ij}\}$ for the process are defined by:

$$\mu = \lim_{t\to\infty} \frac{1}{t} E(X_t) \tag{1}$$

$$\Sigma_{ij} = \lim_{t\to\infty} \frac{1}{t}[E(X_t^i X_t^j) - E(X_t^i)E(X_t^j)], \tag{2}$$

assuming the limits exist, where $E(\cdot)$ always denotes expectation. In the case of unblocked diffusion (no obstacles), $\mu = 0$, $\Sigma_{ij} = I$, the identity matrix, and X_t is a standard Brownian motion ($D = \frac{1}{2}$). The probability density $p(t, x)$ is the function of time and space variables $x \in R^m$ so that

$$P\{X_t \in A\} = \int_A p(t, x)\, dx$$

for any set A where $P\{\cdot\}$ always denotes probability. In the unblocked case, $p(t, x)$ satisfies the heat equation

$$\frac{\partial}{\partial t} p(t, x) = \frac{1}{2} \nabla^2 p(t, x) \tag{3}$$

with initial condition $p(0, x) = \delta(x)$ if $X_0 = 0$.

If $\mathcal{O}$ is a closed set in $\mathbf{R}^m$ with piecewise smooth boundary, B, let X_t denote the coordinates of a Brownian particle diffusing in $\mathcal{O}^c$, the complement of $\mathcal{O}$, and reflected off B. Assume that the diffusion starts at $x = 0$, which is not in $\mathcal{O}^c$ (the diffusion coefficient, which is a long time average, does not depend on the starting point, but choosing $x = 0$ makes the calculation easier). Then, if $p_{\mathcal{O}}(t,x)$ denotes the probability density for the diffusion with obstacle, $\mathcal{O}$, $p_{\mathcal{O}}(t, x)$ satisfies:

$$(i)\ \frac{\partial}{\partial t} p_{\mathcal{O}}(t, x) = \frac{1}{2} \nabla^2 p_{\mathcal{O}}(t, x), \qquad x \in \mathcal{O}^c$$

$$(ii)\ p_{\mathcal{O}}(0, x) = \delta(x)$$

$$(iii)\ \frac{\partial}{\partial n} p_{\mathcal{O}}(t, x) = 0, \quad x \in B$$

where n represents the unit normal to B. The vector $\mu^{\mathcal{O}}$ of effective drifts in the m axial directions and the diffusion matrix, Σ, are given by the probabilistic expressions 1 and 2 but in general, it is extremely difficult to compute what these limits are. However, an analysis can be carried out when $\mathcal{O}$ consists of periodic repetitions of a standard obstacle.

Let the obstacle sets $\mathcal{O}_0$, $\mathcal{O}_1$, $\mathcal{O}$, the unit cube Q, the fundamental region R, the boundary B and the faces C_i be as described in the Methods section, except that we drop the hypothesis that $\mathcal{O}_0$ is invariant under rotations of 90°. Since $\mathcal{O}$ is symmetric about zero and $X_0 = 0$,

$$E(X_t) = 0, \qquad \text{for all } t$$

$$E(X_t^i X_t^j) = 0 \qquad \text{for all } t \text{ and } i \neq j.$$

Thus $\mu^{\mathcal{O}} = 0$ and $\Sigma_{ij}^{\mathcal{O}} = 0$ for $i \neq j$, so we need only compute

$$d_i = \Sigma_{ii}^{\mathcal{O}}$$

the effective diffusion rate in each axial direction to characterize μ and Σ_{ij} completely.

Theorem: Let $\vec{n} = (n_1, \ldots, n_m)$ be the unit normal of R pointing outward. For each i, let u_i be the steady-state solution of the heat equation on R with the following boundary conditions

$$(a)\ \nabla^2 u_i(x) = 0 \qquad x \in R$$

$$(b)\ \frac{\partial u_i(x)}{\partial n} = n_i(x) \quad x \in B_1$$

$$(c)\ u_i(x) = 0 \qquad x \in C_i$$

$$(d)\ \frac{\partial u_i}{\partial n} = 0 \qquad x \in C_j, j \neq i$$

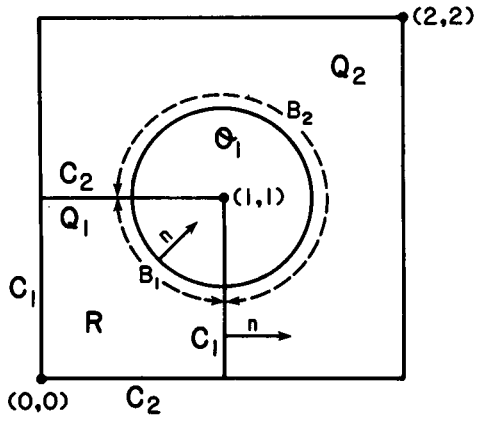

FIGURE 10 Sets used in the proof of the theorem. Regions used in the proof of Eq. 4 of Appendix 1 for the special case of an array of circular obstacles in two dimensions. For further details, see text.

Then

$$d_i = 1 - (\mathrm{vol}(R))^{-1} \int_{B_1} u_i n_i \, ds \tag{4}$$

Sketch of proof: Let Q_2 denote the cube $\{\vec{x} | 0 \le x_i \le 2\}$ and let B_2 be the boundary of the obstacle $\mathcal{O}_1$ in Q_2 but not in Q_1. Denote the boundary of $\mathcal{O}$, the two-periodic extension of $\mathcal{O}_1$ to $\mathbf{R}^m$ by B. Thus B_2 is the part of B in Q_2 and B_1 is the part of B in Q_1 (Fig. 10). For simplicity, denote $P_{\mathcal{O}}(t, x)$ by $p_t(x)$.

By definition

$$\begin{aligned} d_i &= \lim_{T\to\infty} \frac{1}{T} E((X_T^i)^2) \\ &= \lim_{T\to\infty} \frac{1}{T} \left\{ \int_0^T \frac{d}{dt} [E((X_t^i)^2)] \, dt + E((X_0^i)^2) \right\} \\ &= \lim_{T\to\infty} \frac{d}{dt} [E((X_t^i)^2)]_{t=T}, \end{aligned} \tag{5}$$

assuming the limit exists. To compute this limit, note first that

$$\begin{aligned} \frac{d}{dt} E((X_t^i)^2) &= \frac{d}{dt} \int_{\mathbf{R}^m\setminus\mathcal{O}} x_i^2 p_t(x) \, dx \\ &= \int_{\mathbf{R}^m\setminus\mathcal{O}} x_i^2 \frac{d}{dt} p_t(x) \, dx \\ &= \frac{1}{2} \int_{\mathbf{R}^m\setminus\mathcal{O}} x_i^2 \nabla^2 p_t(x) \, dx \end{aligned}$$

by (i). Here and below, $\mathbf{R}^m\setminus\mathcal{O}$ denotes the points in $\mathbf{R}^m$ which are not in $\mathcal{O}$. Using Green's identity one obtains:

$$\begin{aligned} \frac{d}{dt} E((X_t^i)^2) = \int_{\mathbf{R}^m\setminus\mathcal{O}} p_t(x) \, dx - \frac{1}{2} \int_B \frac{d}{dn} (x_i^2) p_t(x) \, ds \\ + \frac{1}{2} \int_B x_i^2 \frac{d}{dn} (p_t(x)) \, ds. \end{aligned}$$

A simple calculation shows that $d/dn(x_i^2) = 2n_i x_i$ and (iii) gives $d/dn\,(p_t(x)) = 0$. Furthermore, $\int_{\mathbf{R}^m\setminus\mathcal{O}} p_t(x) \, dx = 1$. Thus

$$\frac{d}{dt} E((X_t^i)^2) = 1 - \int_B n_i x_i p_t(x) \, dx \tag{6}$$

We now use periodicity. We will write

$$y \sim x \qquad \text{if } y = x + (2j_1, \ldots, 2j_m)$$

for some integers $j_1, \ldots, j_m$

and define

$$q_t(x) = \sum_{y\sim x} p_t(y), \quad x \in Q_2\setminus\mathcal{O}_1.$$

Then, using only periodicity, the following can be proven:

(iv) $\lim_{t\to\infty} q_t(x) = \mathrm{vol}(Q\setminus\mathcal{O})$.

(v) $\lim_{t\to\infty} \frac{d}{dt} \left[\sum_{y\sim x} y_i p_t(y) \right] = 0$.

(vi) $\lim_{t\to\infty} \left[\sum_{y\sim x} y_i p_t(y) \right]$ exists.

We define $\phi_i(x)$ to be the limit in (vi). We will see below that u_i is a scalar multiple of ϕ_i. Using (vi) in Eq. 5, we have

$$\lim_{t\to\infty} \frac{d}{dt} E((X_t^i)^2 = 1 - \int_{B_1} n_i(x) \phi_i(x) \, dx,$$

which expresses d_i in terms of an integral over the obstacle boundary in the unit cell. What equation does $\phi_i(x)$ satisfy? Note that

$$\begin{aligned} \nabla^2 \left(\sum_{y\sim x} y_i p_t(y) \right) &= \sum_{y\sim x} \nabla^2 (y_i p_t(y)) \\ &= \sum_{y\sim x} \frac{\partial}{\partial y_i} [p_t(y)] + \sum_{y\sim x} y_i \nabla^2 p_t(y) \\ &= \frac{\partial}{\partial y_i} [q_t(x)] + 2 \frac{\partial}{\partial t} [\sum_{y\sim x} y_i p_t(y)]. \end{aligned}$$

The first term goes to zero as $t \to \infty$ by (iv) and the second term goes to zero by (v). Therefore $\phi_i(x)$ satisfies

$$\nabla^2 \phi_i(x) = 0 \quad \text{on } Q_2\setminus\mathcal{O}_1. \tag{7}$$

For $x \in B_2$, we find

$$\begin{aligned} \frac{\partial}{\partial n} \left[\sum_{y\sim x} y_i p_t(y) \right] &= \sum_{y\sim x} \frac{\partial}{\partial n} [y_i p_t(y)] \\ &= \sum_{y\sim x} \frac{\partial y_i}{\partial n} p_t(y) \\ &= \frac{\partial x_i}{\partial n} q_t(x) \\ &= n_i(x) q_t(x). \end{aligned}$$

Taking the limit as $t \to \infty$, we obtain

$$\frac{d}{dn} \phi_i(x) = (\mathrm{vol}\,(Q_2\setminus\mathcal{O}_1)) n_i(x), \qquad x \in B_2. \tag{8}$$

Note that ϕ_i is antisymmetric in x_i and symmetric in x_j for $j \neq i$. This,

combined with the assumed invariance of the obstacle under reflections along the coordinate directions implies that:

$$\frac{\partial \phi_i(x)}{\partial n} = 0 \qquad x \in C_j, j \neq i. \tag{9}$$

$$\phi_i(x) = 0 \qquad x \in C_i. \tag{10}$$

Finally, noting that $\mathrm{vol}(R) = 2^{-m}\,\mathrm{vol}(Q_2 \backslash \mathcal{O}_1)$, setting $u_i(x) = [2^m\,\mathrm{vol}(R)]^{-1}\,\phi_i(x)$ gives the result of the theorem by using Eqs. 5 and 6. The properties of u_i are given by Eqs. 7–10.

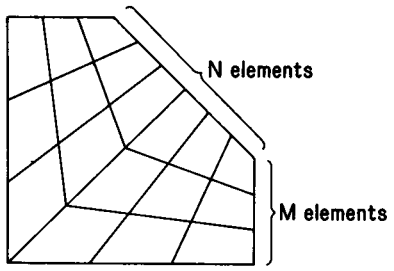

FIGURE 12 Arrangement of finite elements for a two-dimensional region. The finite elements for the calculation on the domain R of Fig. 11 are shown. They are arranged so that all sides and the center diagonal are divided into segments of equal length.

APPENDIX 2

Numerical methods

In this appendix we describe the methods used to solve the Laplace equation (with associated boundary conditions) and to compute the integral for D_g given in the theorem in Methods. We will also indicate the methods by which we validated the accuracy of our numerical techniques.

The Laplace equation was solved using finite element techniques. A two-dimensional example of the region R and the boundary conditions for the Laplace equation is indicated in Fig. 11. In Fig. 12 we show how the finite elements were chosen. The grid is specified by giving the integers N and M and specifying that the central diagonal as well as the sides should be equally divided by the elements. The finite element analysis program (FEAP), originally written by Professor R.L. Taylor of the University of California at Berkeley, was used on a Hewlett-Packard Vax 11-750 computer with VMS operating system to find the solution, w, of the Laplace equation. FEAP is available on floppy diskette for IBM personal computers with PC-DOS 2.0 or higher and on Vax 11-750. Code was written in the language C for computing the integral expression for D_g in terms of w. For the integration the generalized trapezoidal rule was used.

In the three-dimensional case the automatic mesh generation capabilities of the Fortran routine INGRID was used to avoid the hand specification of nodal point coordinates. The trapezoidal boxes for the finite element method were generated by dividing the edges of the faces of the cube and the surfaces B_1 into equal parts as indicated in Fig. 13 for the case of beams with diamond-shaped cross sections. Once P and Q are given the entire mesh is determined. A finite element heat conduction code, TOPAZ, was used in the three-dimensional case to find w and then the trapezoidal rule was used to compute the surface integrals in the expression for D_g. INGRID and TOPAZ are included in a set of programs written at Lawrence Livermore National Laboratory, CA. Memory requirements are 554 KB for INGRID and 116 KB for TOPAZ.

In the two-dimensional case, to solve the problem of circular obstacles with 451 nodes ($c = 0.5$, $M = 10$, and $n = 40$), the CPU time was 34 s. For diamond-shaped obstacles with 341 nodes ($c = 0.5$, $M = 10$, and $N = 30$), it was 26 s. For three-dimensional beams with diamond-shaped cross-sections and 2107 nodes ($c = 0.5$, $P = 4$, and $Q = 9$), the CPU time to run TOPAZ was 10 min.

The accuracy of these numerical calculations was checked in several different ways. First of all, if one changes the boundary conditions appropriately then an analytical solution can easily be derived. This analytical solution can be directly compared with a numerical solution of the same modified problem. In the two-dimensional case, we changed the boundary condition on $x_2 = 1$ from $w = 0$ to $w = 1$. The modified problem has the analytical solution $w = x_1$. Denote the numerical solution of the same problem by u. Then, in the two-dimensional case for diamond-shaped obstacles, for $c = 0.1$, the mesh with $M = 10$ and $N = 30$ gave $w - u < 0.0005$. For $c = 0.5$, the mesh with $M = 10$ and $N = 30$ gave $w - u < 0.0009$. For $c = 0.9$, the mesh with $M = 10$ and $N = 60$

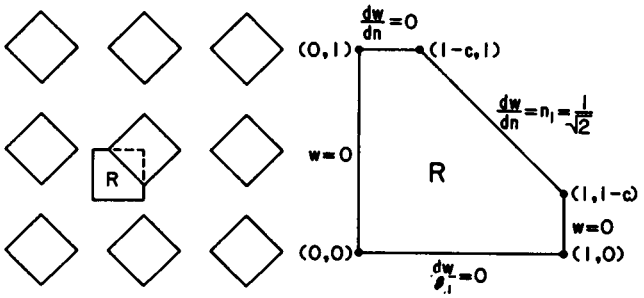

FIGURE 11 Example of a two-dimensional region on which the Laplace equation is solved. A portion of a periodic lattice comprised of diamond-shaped obstacles is shown on the left. The region R is enlarged and boundary conditions are shown on the right.

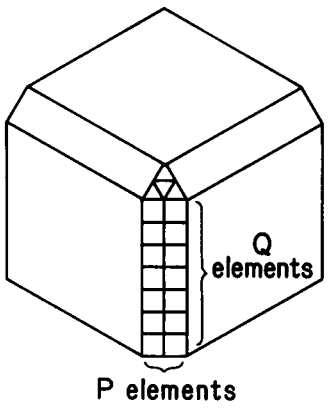

FIGURE 13 Arrangement of finite elements for a three-dimensional region. The finite elements on the boundary B_1 are shown for the case of three-dimensional beams with diamond-shaped cross sections.

TABLE 1 Computed values of D_g for different mesh sizes in the two-dimensional case of diamond-shaped obstacles

C	M	N	D_g
0.1	5	20	0.995
	10	30	0.995
0.5	5	20	0.871
	10	30	0.863
0.9	10	30	0.580
	10	60	0.573
0.99	10	30	0.359
	10	60	0.354

TABLE 2 Computed values of D_g for different mesh sizes in the three-dimensional case of beams with diamond-shaped cross sections

C	P	Q	D_g
0.1	2	5	0.990
	2	9	0.990
0.5	4	5	0.753
	4	10	0.750
0.9	4	5	0.367
	6	5	0.356
0.99	4	5	0.263
	6	5	0.250

gave $w - u < 0.002$. In the three-dimensional case of beams with diamond-shaped cross section various choices of P, Q, and c ($P = 2$, $Q = 10$, and $c = 0.1$; $P = 4$, $Q = 9$, and $c = 0.5$; $P = 6$, $Q = 5$, and $c = 0.9$) all gave $u - w < 0.0001$.

The second method of checking the accuracy of the calculations was to refine the grid and observe the change in the computed value of D_g. The results for different grids for the regions depicted in Figs. 12 and 13 are shown in Tables 1 and 2, respectively. Relatively little change in D_g resulted from these changes in mesh size. Thirdly, one can prove analytically that D_g should approach 0.5 in the two-dimensional case of square obstacles and should approach 0.33 in the three-dimensional case of beams with square cross-section as the critical dimension is reached. These limits were in fact attained to high accuracy in the numerical computations, see Figs. 4–7.

The authors are grateful to Professor Kimon Angelides for sharing with them his unpublished data.

This work was partially supported by National Science Foundation grants DMS-87-01807 to M. Reed and DMS-87-02879 to G. Lawler and an Alfred P. Sloan research fellowship to G. Lawler. The calculations were carried out on the facilities of the National Biomedical Simulation Resources at Duke University.

Received for publication 20 March 1989 and in final form 28 July 1989.

REFERENCES

Derrida, B. 1983. Velocity and diffusion constant for a one-dimensional hopping model. *J. Stat. Phys.* 31:433–450.

Derrida, B., and J. M. Luck. 1983. Diffusion on a random lattice: weak-disorder expansion in arbitrary dimension. *Phys. Rev. B Condens. Matter.* 28:7183–7190.

Ellisman, M. H., and K. R. Porter. 1980. Microtrabecular structure of the axoplasmic matrix: visualization of the cross-linking structures and their distribution. *J. Cell Biol.* 87:464–479.

Fath, K. R., and R. J. Lasek. 1988. Two classes of actin microfilaments are associated with the inner cytoskeleton of axons. *J. Cell Biol.* 107:613–621.

Gershon, N. D., K. R. Porter, and B. L. Trus. 1983. *In* Biological Structures and Coupled Flows. A. Oplatka and M. Balaban, editors. Academic Press, Inc., New York. 377–380.

Gershon, N. D., K. R. Porter, and B. L. Trus. 1985. The cytoplasmic matrix: its volume and surface area and the diffusion of molecules through it. *Proc. Natl. Acad. Sci. USA.* 82:5030–5034.

Gross, G. W., and D. G. Weiss. 1982. Theoretical considerations on rapid transport in low viscosity axonal regions. *In* Axoplasmic Transport, D. G. Weiss, editor, Springer-Verlag, Inc., New York. 330–341.

Jacobson, K., and J. Woijcieszyn. 1984. The translational mobility of substances within the cytoplasmic matrix. *Proc. Natl. Acad. Sci. USA.* 81:6747–6751.

Kempner, E. S., and J. H. Miller. 1968. The molecular biology of *Euglena gracilis*. V. Enzyme localization. *Exp. Cell. Res.* 51:150–156.

Luby-Phelps, K., P. E. Castle, D. L. Taylor, and F. Lanni. 1987. Hindered diffusion of inert tracer particles in the cytoplasm of mouse 3T3 cells. *Proc. Natl. Acad. Sci. USA.* 84:4910–4913.

Luby-Phelps, K., F. Lanni, and D. L. Taylor. 1988. The submicroscopic properties of cytoplasm as a determinant of cellular function. *Annu. Rev. Biophys. Biophys. Chem.* 17:369–396.

Luby-Phelps, K., and D. L. Taylor. 1988. Subcellular compartmentalization by local differentiation of cytoplasmic structure. *Cell Motil. Cytoskeleton.* 10:28–37.

Luby-Phelps, K., D. L. Taylor, and F. Lanni. 1986. Probing the structure of cytoplasm. *J. Cell. Biol.* 102:2015–2022.

Mastro, A. M., M. A. Babich, W. D. Taylor, and A. D. Keith. 1984. Diffusion of a small molecule in the cytoplasm of mammalian cells. *Proc. Natl. Acad. Sci. USA.* 81:3414–3418.

Muramatsu, N., and A. P. Minton. 1988. Tracer diffusion of globular proteins in concentrated protein solutions. *Proc. Natl. Acad. Sci. USA.* 85:2984–2988.

Rayleigh, Lord. 1982. On the influence of obstacles arranged in rectangular order on the properties of a medium. *Philos. Magnet. Ser. 5.* 34:481–502.

Renkin, E. M. 1955. Filtration, diffusion, and molecular sieving through porous cellulose membranes. *J. Gen. Physiol.* 38:225–243.

O'Leary, T. 1987. Concentration dependence of protein diffusion. *Biophys. J.* 52:137–139.

Saxton, M. J. 1987. Lateral diffusion in an archipelago. The effect of mobile obstacles. *Biophys. J.* 52:989–998.

Saxton, M. J. 1989. The spectrin network as a barrier to lateral diffusion in erythrocytes. A percolation analysis. *Biophys. J.* 55:21–28.

Vanninanthan, M. 1981. Homogenization of eigenvalue problems in perforated domains. *Proc. Indian Acad. Sci. Math. Sci.* 90:239–271